Article:
Pakzad, Sina Zare, Esfahani, Mohammad Nasr and Erdem Alaca, B. (2024) Investigation of the Bending Behavior in Silicon Nanowires: A Nanomechanical Modeling Perspective. International Journal of Applied Mechanics. 2450073. ISSN: 1758-826X

https://doi.org/10.1142/S175882512450073X

International Journal of Applied Mechanics

Investigation of the Bending Behavior in Silicon Nanowires: A Nanomechanical Modeling Perspective

Sina Zare Pakzad
Department of Mechanical Engineering, Koç University, Rumelifeneri Yolu, 34450 Sariyer, Istanbul, Turkey

Mohammad Nasr Esfahani
School of Physics, Engineering and Technology, University of York, York, YO10 5DD, UK

B. Erdem Alaca*
Department of Mechanical Engineering, Koç University, Rumelifeneri Yolu, 34450 Sariyer, Istanbul, Turkey

n^2STAR-Koç University Nanofabrication and Nanocharacterization Center for Scientific and Technological Advanced Research, Koç University, Rumelifeneri Yolu, 34450 Sariyer, Istanbul, Turkey

Koç University Surface Technologies Research Center (KUYTAM), Koç University, 34450 Sariyer, Istanbul, Turkey

Received date
Accepted date

Nanowires play a crucial role across a wide range of disciplines such as nanoelectromechanical systems, nanoelectronics, and energy applications. As nanowires continue to reduce in dimensions, their mechanical properties are increasingly affected by surface attributes. This study conducts a comprehensive examination of nanomechanical models utilized for interpreting large deformations in the bending response of silicon nanowires. Specifically, the Heidelberg, Hudson, Zhan, SimpZP, and ExtZP nanomechanical models are explored regarding their capability to predict the elastic properties of silicon nanowires with varying critical dimensions and crystal orientations. Molecular dynamics simulations are employed to model silicon nanowires with unreconstructed surface states. The calculation of intrinsic stresses and the methodology for quantifying surface properties, including surface stresses and surface elasticity constants, are carried out using atomistic modeling. The findings reveal significant disparities of up to 100 GPa among nanomechanical models in interpreting a singular force-deflection response obtained for a silicon nanowire. Inadequate consideration of surface and intrinsic effects in nanomechanical modeling of nanowires leads to substantial variability in their mechanical properties. This investigation yields valuable insights into the surface characteristics of silicon nanowires, thereby enhancing our understanding of the essential role played by nanomechanical models in the intricate interpretation of mechanical properties at the nanoscale.

Keywords: Silicon; Nanowire; Nanomechanical Modeling; Bending; Molecular Dynamics;

*Corresponding author.

Surface Stress; Surface Elasticity.

1. Introduction

Nanowires (NWs) hold great promise as fundamental components for advancing future nanoelectromechanical systems [Bachtold *et al.*, 2022], nanoelectronics [Li *et al.*, 2023], [Zhang *et al.*, 2021], with notable applications in highly sensitive sensors [Karimzadehkhouei *et al.*, 2023], [Akbari *et al.*, 2020], [Maita *et al.*, 2023] and cutting-edge energy technologies [Panda *et al.*, 2022]. The remarkable advancements in fabrication methods [Wang *et al.*, 2016], [Liang *et al.*, 2023], technological applicability [Alaca & Karimzadehkhouei, 2023], and multi-scale modeling techniques [Momeni *et al.*, 2020], [Zare *et al.*, 2023a], [Zare Pakzad *et al.*, 2023b] have sparked great interest in the extensive characterization of NWs. The miniaturization of NWs leads to a significant increase in the ratio of surface area to volume giving rise to remarkable physical properties distinguishing them from bulk structures [Nasr Esfahani & Alaca, 2019], [Wang *et al.*, 2017], [Huang *et al.*, 2023]. In this context, the surface properties of NWs assume a notably significant role and are regarded as pivotal factors that influence their mechanical attributes[Muller *et al.*, 2004], [Zare Pakzad *et al.*, 2023a], [Zare Pakzad *et al.*, 2023b]. Furthermore, intrinsic effects such as the stresses generated in NWs during fabrication, assembly, and surface interactions are recognized as dominant parameters that have significant effects on the performance and properties of NWs [Zare *et al.*, 2023b], [Nasr Esfahani *et al.*, 2022], [Fedorov *et al.*, 2019], [Li *et al.*, 2021], [Urena *et al.*, 2013], [Yokogawa *et al.*, 2017], [Lorenzoni *et al.*, 2016], [Dolabella *et al.*, 2020], [Spejo *et al.*, 2020] Nanomechanical modeling techniques are developed as a means to interpret the behavior of NWs at the nanoscale. The classical surface elasticity theory proposed by Gurtin and Murdoch [1975] has found extensive application in studying the size-dependent mechanical properties of NWs. As dimensions are further scaled down, various surface models are incorporated into nanomechanical modeling approaches in an attempt to elucidate the deformation behavior at the nanoscale regime [He & Lilley, 2008], [Song *et al.*, 2011], [Chen *et al.*, 2006]. In this regard, different formulations of the Young-Laplace model (YL) have been utilized in numerous studies to interpret the properties of NWs. These include the original formulation of YL [Chen *et al.*, 2006], the modified YL [He & Lilley, 2008], [Zare *et al.*, 2021b], and the extended YL [Song *et al.*, 2011], [Zare Pakzad *et al.*, 2023b]. Furthermore, various core-shell models have been developed as structural frameworks that comprise a core with the modulus of the bulk material and a surface shell [Yao *et al.*, 2012], [Xu *et al.*, 2016], [Xiao *et al.*, 2022]. These models are utilized to interpret and analyze the impact of surface properties on the overall behavior of the NWs [Li *et al.*, 2022], [Miller and Shenoy, 2000], [Zare Pakzad *et al.*, 2023a]

Silicon (Si) NWs have been extensively investigated as fundamental components in semiconductor manufacturing due to their unique properties [Nasr Esfahani & Alaca, 2019], [Wang *et al.*, 2017], [Ye *et al.*, 2019]. Despite numerous studies on the

size-dependent mechanical properties of Si NWs, conflicting reports have led to the need for a more detailed examination of the scale effect [Zare Pakzad *et al.*, 2023a], [Zare Pakzad *et al.*, 2023b], [Yang *et al.*, 2022]. Specifically, the size-dependent modulus of elasticity of Si NWs has been addressed using various computational and experimental methods, resulting in discrepancies regarding the scale effect [Nasr Esfahani & Alaca, 2019], [Yang *et al.*, 2022]. The importance of nanomechanical model selection is highlighted in a recent study, where deviations of up to 85 GPa are attributed to the specific choice of the model [Zare Pakzad *et al.*, 2023b]. Considering the challenges in fabrication, testing, and characterization, modeling remains a critical step in the successful interpretation of results [Zare Pakzad *et al.*, 2021a], [Zare Pakzad *et al.*, 2023b], [Zare Pakzad *et al.*, 2023c], [Zare Pakzad *et al.*, 2023d], [Pakzad *et al.*, 2024]. The use of bending experiments, aided by advancements in testing methods and *in-situ* approaches, has gained significant importance in revealing the properties of Si NWs [Espinosa *et al.*, 2013]. Within this framework, the development of nanomechanical models that account for large deflections observed in Si NWs has been ongoing [Heidelberg *et al.*, 2006], [Ngo *et al.*, 2006], [Zare Pakzad *et al.*, 2023b], [Zare Pakzad *et al.*, 2021a]. Previous nanomechanical models, such as those proposed by Heidelberg *et al.* [2006] for large deflection due to axial extension, extended with initial tension effects by Hudson *et al.* [2013], incorporating surface effects based on modified YL model by Zhan *et al.* [2012], and combined effects by Zare Pakzad *et al.* [2021a], make this research area particularly intriguing for further exploration. Introducing the ExtZP model [Zare Pakzad *et al.*, 2023b], the recent multi-scale approach presents a comprehensive formulation that accounts for large deflections, incorporates anisotropic surface properties using the extended YL model, and considers intrinsic terms encompassing effects arising from surface and initial tension conditions. Moreover, the modeling of the surface properties goes beyond mathematical formulation and also requires an examination of surface state and orientation-dependent properties, such as surface stress and surface elasticity constants. Moreover, recent studies by Zare Pakzad *et al.* [Zare Pakzad *et al.*, 2021b], [Zare Pakzad *et al.*, 2023b] propose a reliable approach to compare unreconstructed and native oxide surface states for (100)- and (110)-Si surfaces. As surface effects continue to gain significance, molecular dynamics (MD) and density functional theory (DFT) simulations are playing vital roles in revealing the size-dependent trends in the elastic properties of Si NWs [Zare Pakzad *et al.*, 2023a], [Zare Pakzad *et al.*, 2021b], [Lee & Rudd, 2007], [Pakzad *et al.*, 2024]. In line with this, MD simulations are used to subject Si NWs to tensile [Xu & Kim, 2019], [Kang *et al.*, 2007], [Zare Pakzad *et al.*, 2023a], [Zare Pakzad *et al.*, 2023b], vibrational [Kim *et al.*, 2006], [Park *et al.*, 2005], and bending tests [Zhuo & Beom, 2018], [Ilinov & Kuronen, 2014], providing valuable insights into their mechanical properties.

The objective of this investigation is to explore the elastic characteristics of Si NWs by employing nanomechanical modeling, taking into account the surface

properties for a range of dimensions and crystallographic orientations. Different nanomechanical models are employed to estimate the mechanical properties based on the force-deflection response of Si NWs, thereby facilitating an examination of large deflection in the bending deformation witnessed in three-point bending tests. The surface properties of Si are computed based on a thin film model for differing crystal orientations, which are used in the nanomechanical models considering the surface effects. Findings here assess the efficacy of different nanomechanical models and establish a multi-scale framework for introducing a strategy to probe the size-dependency of Si NW properties, with particular emphasis on unreconstructed surface states. Through this study, valuable insights are obtained on the surface characteristics of Si NWs. In this context, this study lays the groundwork for parallel integration of intrinsic and surface stresses into advanced nanomechanical modeling, underscoring the significance of investigating multiscale theoretical frameworks for characterizing the mechanical properties of Si NWs.

2. Materials and Methods

This section encompasses four segments, which focus on the methods used to interpret the selection of nanomechanical models and their effects on the calculated elastic responses of Si NWs. These include the analytical constitution of the models, formulations for effective bending rigidity, three-point bending simulations of Si NWs using MD, and atomistic simulations of surface properties. The methods are utilized to interpret the elastic response of Si NWs with varying sizes and crystal orientations through different nanomechanical models. The order in which these methods are described is as follows: Section 2.1 provides details about the existing nanomechanical models employed to interpret the bending response in NWs. Section 2.2 discusses the integration of effective modulus of elasticity definitions into the models, along with their respective formulations that incorporate surface analogy, elucidating the bending rigidity details. Section 2.3 delves into the bending simulations performed on Si NWs via MD method. Finally, Section 2.4 presents the atomistic method employed to calculate surface properties (surface stress and surface elasticity constants) for different orientations of unreconstructed Si film.

2.1. *Nanomechanical Models*

The section begins by introducing the Heidelberg model, which represents the most general version of large deflection models utilized in the interpretation of bending deformations in NWs [Heidelberg *et al.*, 2006]. Following that, Section 2.1.2 introduces an extended version of the Heidelberg model called the Hudson model [Hudson *et al.*, 2013], which incorporates intrinsic stress induced by initial tension/compression. In Section 2.1.3, Zhan *et al.*'s modification of the Heidelberg model [Zhan & Gu, 2012] is discussed, including the modified YL surface model to incorporate surface properties. Section 2.1.4 explains the large deflection model proposed by Zare Pakzad

et al. [Zare Pakzad *et al.*, 2021a], referred to as SimpZP. This model incorporates both intrinsic stress induced by initial tension/compression and the modified YL surface model. Finally, in Section 2.1.5, a recently developed nanomechanical model, known as the ExtZP model [Zare Pakzad *et al.*, 2023b], is presented. It integrates the extended YL model and intrinsic stresses induced by both surface effects and initial tension/compression. These nanomechanical models enable the prediction of the modulus of elasticity (E) for Si NWs by employing different sets of parameters as inputs. Fig. 1 (a) provides an overview, schematically illustrating the effective parameters associated with each model, including large deflection, intrinsic stress, and surface properties.

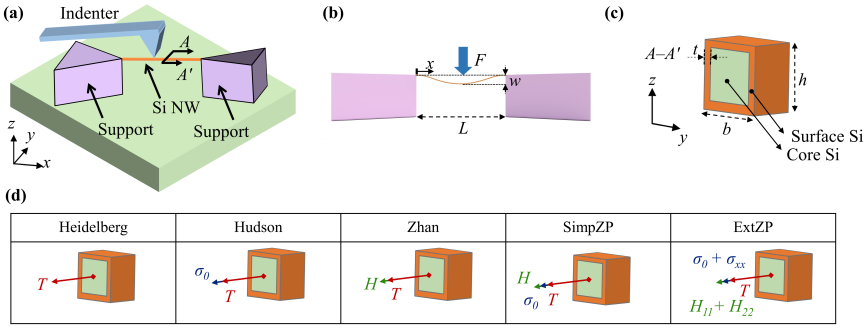

Fig. 1. (a) Schematic representation of Si NW, clamped by support regions and subjected to the force applied by an indenter. (b) Schematic of a NW of length L under bending test with applied load F, and subsequent deformation w at its center. (c) Cross-sectional representation of the NW with associated height (h), width (b), and surface layer thickness (t). (d) Effective terms of different nanomechanical models are presented.

2.1.1. *Heidelberg Model*

The Heidelberg model [Heidelberg *et al.*, 2006] presents the most general method for interpreting the bending behavior of Si NWs when subjected to large deformation during a three-point bending test. The governing equation for a NW of length L and of rectangular cross section loaded at its midsection by a point load F (Fig. 1 (a)) is given in Eq. 1.

$$EI\frac{\partial^4 w}{\partial x^4} - T\frac{\partial^2 w}{\partial x^2} = \frac{F}{2}\big(-\delta(x) + 2\delta(x - \frac{L}{2}) - \delta(x - L)\big) \tag{1}$$

In Eq. 1, w represents the transversal displacement in the z-direction, x denotes the longitudinal axis of the beam, I represents the moment of inertia, T signifies the overall tension along the NW, and δ is the Dirac delta function, as depicted in Fig. 1 (b). The first term in Eq. 1 arises from the bending of the beam, while the second term is associated with the stretching along the axial direction of the beam,

often referred to as large deflection in nanomechanics. The axial tension term can be expressed as Eq. 2.

$$T = \frac{EA}{2L}\int_0^L (\frac{\partial w}{\partial x})^2 dx \tag{2}$$

By integrating Eq. 1 and Eq. 2 with respect to x, and taking into account the usual clamped boundary conditions (B.C.s) at both ends of the NW, as well as the cross-sectional area denoted as A, Eq. 3 is obtained.

$$F = \frac{192EI}{L^3} w(\frac{L}{2}) f(\alpha) \tag{3}$$

Eq. 3 is commonly known as the linear beam deflection approximation, with the relationship $f(\alpha) = 1$. However, when a precise solution method is employed, the function $f(\alpha)$ yields Eq. 4.

$$f(\alpha) = \frac{\alpha}{48 - \frac{192\tanh(\sqrt{\alpha}/4)}{\sqrt{\alpha}}} \tag{4}$$

The value of α, which is connected to the maximum deflection through Eq. 5 is utilized to calculate $f(\alpha)$ in order to predict the modulus of elasticity of Si NWs using Heidelberg model.

$$\big(\frac{\alpha\cosh^2(\frac{\sqrt{\alpha}}{4})}{2+\cosh(\frac{\sqrt{\alpha}}{2}) - 6\frac{\sinh(\frac{\sqrt{\alpha}}{2})}{\sqrt{\alpha}}}\big)\big(1 - 4\frac{\tanh(\sqrt{\alpha}/4)}{\sqrt{\alpha}}\big)^2 = \Delta Z^2_{center}\big(\frac{E}{I}\big) \tag{5}$$

2.1.2. *Hudson Model*

According to the Hudson model [Hudson *et al.*, 2013], in order to analytically include residual stresses resulting from initial tension/compression into the Heidelberg model, it is essential to incorporate the term T_0, which represents the initial axial force along the NW. This term is added to Eq. 2 with an updated formulation provided in Eq. 6. The Hudson model utilizes a governing equation that is similar to the Heidelberg model, thereby allowing it to account for the effects of embedded initial stresses.

$$T = T_0 + \frac{EA}{2L}\int_0^L (\frac{\partial w}{\partial x})^2 dx \tag{6}$$

The presence of the term T_0 in the formulation signifies the residual term that is embedded within the NW, arising from fabrication or assembly-induced stresses. By solving Eq. 1 and Eq. 6 according to the Hudson model, the exact analytical solution provided in Eq. 7 is derived.

$$(1-\frac{L^2T_0}{\alpha EI})(\frac{EA}{T_0+EA}) \quad \big(\frac{\alpha\cosh^2(\frac{\sqrt{\alpha}}{4})}{2+\cosh(\frac{\sqrt{\alpha}}{2})-6\frac{\sinh(\frac{\sqrt{\alpha}}{2})}{\sqrt{\alpha}}}\big)\times \big(1-4\frac{\tanh(\sqrt{\alpha}/4)}{\sqrt{\alpha}}\big)^2 = \Delta Z^2_{center}\big(\frac{E}{I}\big) \tag{7}$$

It is worth mentioning that an approximate version of Hudson's model is proposed by Yaish *et al.* [2015], where the function $f(\alpha)$ is approximated as Eq. 8.

$$f(\alpha) = 1 + 2.412\times10^{-2}\alpha - 1.407\times10^{-6}\alpha^2 \tag{8}$$

2.1.3. *Zhan Model*

The Zhan model [Zhan & Gu, 2012], which incorporates a surface model based on the modified YL equation, introduces updates to the formulation of the Heidelberg model. These updates are reflected as surface stress and surface elasticity constant given in Eq. 9. As the analytical bending formulation incorporates the surface model, the concept of the effective modulus of elasticity, represented as E^*, becomes necessary. Consequently, all formulations utilizing surface embedded models consider both the effective modulus of elasticity and the effective moment of inertia (I^*). Subsequently, this article will delve into the specifics of the bending rigidity formulation for determining the modulus of elasticity of Si NWs Section 2.2. Eq. 9 shows the governing equation provided by Zhan model.

$$(EI)^*\frac{\partial^4 w}{\partial x^4} - T\frac{\partial^2 w}{\partial x^2} - H\frac{\partial^2 w}{\partial x^2} = \frac{F}{2}\big(-\delta(x) + 2\delta(x-\frac{L}{2}) - \delta(x-L)\big) \tag{9}$$

In Eq. 9, H represents the surface parameter that incorporates the surface stress, f_{11}, and the surface elasticity constant, d_{11} with detailed form given in Eq. 10.

$$H = 2hd_{11}\epsilon_x + 2f_{11}h \tag{10}$$

In Eq. 10, h represents the thickness of the NW, and ϵ_x denotes the axial strain. By solving Eq. 9, following a similar approach as the previous models, the solution given in Eq. 11 is obtained.

$$(1-\frac{2f_{11}hL^2}{\alpha(EI)^*})\big(\frac{\alpha\cosh^2(\frac{\sqrt{\alpha}}{4})}{2+\cosh(\frac{\sqrt{\alpha}}{2})-6\frac{\sinh(\frac{\sqrt{\alpha}}{2})}{\sqrt{\alpha}}}\big) \quad \big(1-4\frac{\tanh(\sqrt{\alpha}/4)}{\sqrt{\alpha}}\big)^2 = \Delta Z^2_{center}\big(\frac{(EA)^*+2d_{11}h}{(EI)^*}\big) \tag{11}$$

In this regard, E^* for the Si NW is derived by numerically solving Eq. 11. The bending rigidity associated with the modified YL model is utilized to predict the modulus of elasticity of the Si NW. Section 2.2 will elaborate on the precise formulation concerning the bending rigidity aligned with Zhan model.

2.1.4. *SimpZP Model*

The SimpZP model [Zare Pakzad *et al.*, 2021a] incorporates both fabrication induced residual stress, σ_0, and surface effects, H, via modified YL formulation. In this context, this model leverages the governing terms outlined in Eq. 12, wherein Eq. 6 replaces Eq. 2 to represent the axial extension term, considering the embedded initial tension/compression component. Essentially, this approach integrates the formulations provided by the Heidelberg, Hudson, and Zhan models, encompassing all the previously discussed terms associated with these models. The solution provided by SimpZP model is given in Eq. 12.

$$(1-\tfrac{L^2T_0}{\alpha(EI)^*})(\tfrac{(EA)^*}{T_0+(EA)^*})(1-\tfrac{2f_{11}hL^2}{\alpha(EI)^*})\big(\tfrac{\alpha\cosh^2(\frac{\sqrt{\alpha}}{4})}{2+\cosh(\frac{\sqrt{\alpha}}{2})-6\frac{\sinh(\frac{\sqrt{\alpha}}{2})}{\sqrt{\alpha}}}\big)\times (1-4\tfrac{\tanh(\sqrt{\alpha}/4)}{\sqrt{\alpha}}\big)^2=\Delta Z^2_{center}\big(\tfrac{(EA)^*+2d_{11}h}{(EI)^*}\big) \tag{12}$$

In accordance with the SimpZP formulation, the bending rigidity formulation derived from the modified YL model is integrated with this model to provide the relation between E and E^*. Similar to Zhan model, in Section 2.2, the specific formulation regarding the bending rigidity, in alignment with the SimpZP model, will be elaborated upon.

2.1.5. *ExtZP Model*

The model proposed by Zare Pakzad *et al.* [2023b], ExtZP model, represents a multiscale extension of prior models, where the treatment of the surface is enhanced by incorporating two new sets of effective parameters: i) anisotropic surface parameters, H_{11} and H_{22}, and ii) surface-induced residual stresses, σ_{xx}. Consequently, the ExtZP approach represents the most comprehensive method for interpreting the bending response of Si NWs. In this approach, Eq. 13 incorporates the surface terms derived from the extended YL surface model, which are combined with the governing equation presented in Eq. 9 and the initial extension term expressed in Eq. 6. In this formulation, b represents the NW width.

$$H=H_{11}+H_{22}+bh\sigma_{xx}=2bf_{11}+2hf_{22}+2bd_{11}+2hd_{22}+bh\sigma_{xx} \tag{13}$$

With terms H_{11} and H_{22} defined as effective surface terms embedding the surface constants and geometrical representation of involved side surfaces [Song*et al.*, 2011] the complete form of ExtZP model can be rewritten as Eq. 14 where $(EI)^*$ represents the effective flexural rigidity. The indices 11 and 22 denote the corresponding directions for the involved planar surfaces.

$$(EI)^* \frac{\partial^4 w}{\partial x^4} - T\frac{\partial^2 w}{\partial x^2} - 2bf_{11}\frac{\partial^2 w}{\partial x^2} - 2hf_{22}\frac{\partial^2 w}{\partial x^2} \\ -2bd_{11}\frac{\partial^2 w}{\partial x^2} - 2hd_{22}\frac{\partial^2 w}{\partial x^2} - bh\sigma_{xx}\frac{\partial^2 w}{\partial x^2} = \\ \frac{F}{2}\big(-\delta(x) + 2\delta(x-\frac{L}{2}) - \delta(x-L)\big) \tag{14}$$

Expanding upon the terms present in Eq. 14, there are five terms that account for surface effects. These terms consist of the surface stress components (f_{11} and f_{22}), surface elasticity constants (d_{11} and d_{22}), and the residual stress induced by the surface (σ_{xx}). The exact solution for the nanomechanical model is given in Eq. 15. Section 2.2 will provide the bending rigidity formulation for the ExtZP model, which is based on the extended YL approach.

$$(1-\frac{L^2T_0}{\alpha(EI)^*})(\frac{(EA)^*}{T_0+(EA)^*})(1-\frac{L^2H_{11}}{\alpha(EI)^*})(1-\frac{L^2H_{22}}{\alpha(EI)^*}) \\ \big(\frac{\alpha\cosh^2(\frac{\sqrt{\alpha}}{4})}{2+\cosh(\frac{\sqrt{\alpha}}{2})-6\frac{\sinh(\frac{\sqrt{\alpha}}{2})}{\sqrt{\alpha}}}\big)\big(1-4\frac{\tanh(\sqrt{\alpha}/4)}{\sqrt{\alpha}}\big)^2 = \\ \Delta Z^2_{center}\big(\frac{(EA)^*+2d_{11}b+2d_{22}h+bhE^*}{(EI)^*}\big) \tag{15}$$

2.2. *Bending Rigidity Calculation*

To estimate the value of E, the connection between classical bending rigidity and effective bending rigidity is employed, which relies on surface properties and geometric definitions. The formulation for the effective bending rigidity, as given by Eq. 16, utilizes a modified YL method [He *et al.*, 2008], [Wang & Feng, 2007] that aligns with the Zhan and SimpZP models.

$$(EI)^* = EI + (E_s)(\frac{bh^2}{2} + \frac{h^3}{6}) \tag{16}$$

In this context, the ExtZP model requires the calculation of the modulus of elasticity, which relies on the effective bending rigidity formulated using the extended YL model [Song*et al.*, 2011], [Zare Pakzad *et al.*, 2023b], as expressed in Eq. 17.

$$(EI)^* = EI + (E_s + \tau_0)(\frac{bh^2}{2} + \frac{h^3}{6}) \tag{17}$$

These formulations designate the average values of surface stresses (f_{11} and f_{22}) and surface elasticity constants (d_{11} and d_{22}) as τ_0 and E_s, respectively. In the field of nanomechanical models, these terms are commonly known as the surface modulus and initial surface stress, as discussed in the literature [He & Lilley, 2008]. More detailed information regarding the formulation of previous models[Heidelberg *et al.*, 2006], [Hudson *et al.*, 2013], [Zhan & Gu, 2012], [Zare Pakzad *et al.*, 2021a], [Zare Pakzad *et al.*, 2023b] and related expressions for bending rigidity [Song *et al.*, 2011], [He & Lilley, 2008], Wang & Feng, 2007] can be found in other sources.

2.3. *Bending Modeling*

Simulations of three-point bending are conducted on double-clamped Si NWs using MD method [Plimpton, 1995]. Fig. 2 illustrates the initial atomic configurations of Si NWs, where the width (h) and height (b) are varied between 2 nm and 5 nm. The Si NWs have a square cross-section, with the width being equal to the height. In this regard, the length (L) of the Si NW remains constant at 600 nm for different critical dimensions. Furthermore, it should be noted that support regions exist on each side of the Si NW and have a length (L_s) of 60 nm. It is crucial to mention that both the length of the NW and the length of the support regions are kept constant across all critical dimensions of the Si NWs. This ensures a length-to-width aspect ratio (AR) greater than 10 for all NW critical dimensions, effectively excluding any potential length-related effects [Zare Pakzad *et al.*, 2023a]. A constant surface layer thickness (t) of 0.5 nm is assumed for all Si NWs studied here. To maintain consistency in cross-section designs and accurate examination of surface constants, it is common to observe rectangular or square geometries in top-down fabricated Si NWs with $< 100 >$ and $< 110 >$ orientations [Nasr Esfahani & Alaca, 2019]. On the other hand, circular cross-sections are frequently encountered in bottom-up fabricated Si NWs with $< 111 >$ and $< 112 >$ orientations [Nasr Esfahani & Alaca, 2019]. In order to maintain consistency in defining the height and thickness of the Si NWs and to accurately analyze surface constants, square cross-sections have been chosen for all four orientations investigated in this study. This decision ensures that the cross-section designs are uniform across the orientations ($< 100 >$, $< 110 >$, $< 111 >$ and $< 112 >$), enabling precise comparisons and comprehensive analysis of the Si NWs. To simulate the clamped B.C., the boundary regions at both ends are fixed in all three dimensions (x, y, and z). The non-periodic shrink-wrapped B.C.s are applied in all directions. The Si NWs undergo a quasi-static relaxation process using the conjugate gradient method to reach a local minimum configuration. Subsequently, a relaxation process is performed on all NWs at a temperature of 1.0 K for 40 ps, utilizing a time step of 1 fs. This is accomplished by employing a canonical NVT ensemble with a Nose-Hoover thermostat. The Tersoff-T3 potential [Tersoff, 1988] as an empirical function composed of two-body terms depending on the local environment is used for the modeling of Si NWs in this work. The associated Si NW stress state, π_{ij}, is calculated using the virial theorem [Zimmerman *et al.*, 2004], given in Eq. 18.

$$\pi_{ij} = \frac{1}{2\Omega_0}\left[\sum_{\alpha=1}^{N}\sum_{\beta\neq\alpha}^{N}\frac{1}{r^{\alpha\beta}}\frac{\partial V(r^{\alpha\beta})}{\partial r}(v_i^{\alpha\beta}v_j^{\alpha\beta})\right] \tag{18}$$

In Eq. 18, Ω_0 stands for the atomic volume in an undeformed system with N as the total number of atoms where associated atomic volume for Si is calculated via relaxation of related structure with further details given in Ref. [Zare Pakzad *et al.*, 2021b]. Atomic distances between atoms α and β are represented as $r_{\alpha\beta}$.

v_j^α stands for the position of atom α along j direction, i.e., $v_j^{\alpha\beta} = v_j^\alpha - v_j^\beta$ and V represents the interatomic potential. The F/w ratio, which is the ratio of force to deflection, can be determined by analyzing the slope of the initial linear section of the force-deflection response. This ratio is often used to estimate the modulus of elasticity through a linear approach. However, it should be noted that in the case of bending response curves for Si NWs, the displacement of the NW upon loading is expected to be larger than half of the cross-sectional size ($h/2$). As a result, the response is likely to exhibit a non-linear behavior, as observed in prior experimental and MD studies on the bending of NWs [Zare Pakzad *et al.*, 2023b], [Zare Pakzad *et al.*, 2021b]. In this context, the nanomechanical models described in Section 2.1 will be utilized to estimate the modulus of elasticity for Si NWs with various crystallographic orientations and critical dimensions.

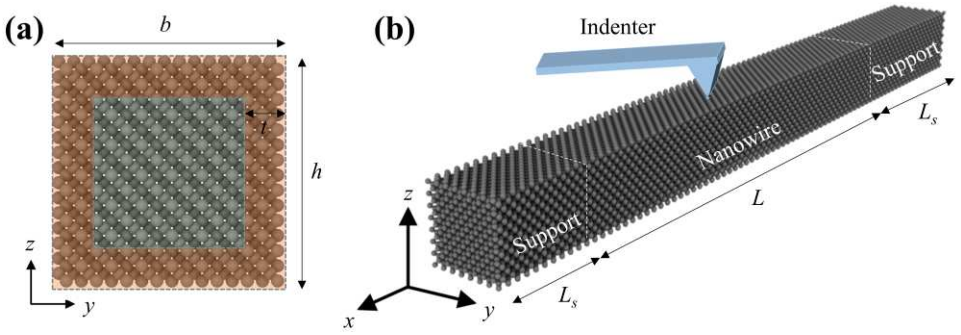

Fig. 2. (a) The initial configuration of Si NW of width, b, height, h, and surface layer thickness, t. (b) The perspective view of a double-clamped NW showing the atomic configuration of a Si NW under 3-point bending simulation using a spherical indenter with associated support regions.The NW length (L) and support region length (L_s) are shown here.

2.4. *Surface Properties Modeling*

Table 1. Dimensions, number of atoms and evaluation areas of unreconstructed Si thin film structures with associated crystallographic orientations.

Structure	Si Orientation			Dimensions [nm]			# of atoms	A_{film}
	x	y	z	x	y	z		(nm^2)
Si (100)	[100]	[010]	[001]	4.35	4.35	4.35	4224	37.8
Si (110)	[$\bar{1}$10]	[001]	[110]	6.15	4.35	6.15	8448	53.5
Si (111)	[$\bar{1}\bar{1}$2]	[1$\bar{1}$0]	[111]	7.10	6.15	7.52	16378	87.3
Si (112)	[1$\bar{1}$0]	[11$\bar{1}$]	[112]	6.15	7.52	7.10	16356	106.8

To quantify the surface stress components (f_{11} and f_{22}) and surface elastic constants (d_{11} and d_{22}) for four orientations of Si NWs, Martin's method can be applied to the thin film structures given in Fig. 3. By employing periodic boundary

conditions in the x- and y-directions, an infinite film model with a finite thickness (L_z) in the z-direction is obtained. The evaluation area (A_{film}) consists of two free surfaces facing each other, and the film must be sufficiently thick to prevent interaction between these two surfaces. The dimensions, crystallographic orientations, numbers of atoms, and evaluation areas are listed in Table 1. The atomic structures are designed to be 8 times the lattice constants of Si along each crystallographic direction. This ensures an appropriate thickness for the film, allowing for accurate calculations of surface stresses and surface elastic constants.

To determine the surface stress components, the structures are initially equilibrated at a temperature of 0.01 K using NPT dynamics. Afterward, the total energy is minimized using the steepest descent and conjugate gradient techniques. The surface stress components are then calculated by assuming a film thickness of L_z, and are formulated according to Eq. 19. In this equation, the parameter η represents the average strain resulting from the relaxation process [Izumi *et al.*, 2004], [Zare Pakzad *et al.*, 2021b], [Zare Pakzad *et al.*, 2023b]. The Tersoff-T3 potential [Tersoff, 1988] is used for the modeling of Si thin films.

$$f_{ij}(\eta) = f_{ij}^{film}(\eta) - f_{ij}^{bulk}(\eta) \tag{19}$$

The estimation of bulk surface stress requires a separate analysis using the bulk model. The surface stress for the film model can be determined by utilizing the stress tensor definition, denoted as σ_{ij}^{film}, as described in Eq. 20. For more comprehensive information regarding the stress tensor of thin films, additional details can be found elsewhere [Izumi *et al.*, 2004], [Zare Pakzad *et al.*, 2021b], [Zare Pakzad *et al.*, 2023b].

$$f_{ij}^{film}(\eta) = \sigma_{ij}^{film}(\eta)\frac{L_z}{2} \tag{20}$$

The surface elastic constants (d_{ijkl}) are defined as the second-order derivatives of surface energy with respect to strain under plane-stress conditions. To calculate the elastic constants for both the bulk (C_{ijkl}^{bulk}) and film (C_{ijkl}^{film}) models, specific considerations are made. For the bulk model, the elastic constants are defined under plane-stress conditions ($C_{ijkl}^{bulk,plane}$), which can be determined using the relationships provided in Eq. 21, Eq. 22, and Eq. 23 [Izumi *et al.*, 2004], [Zare Pakzad *et al.*, 2021b], [Zare Pakzad *et al.*, 2023b].

$$C_{11}^{bulk,plane} = C_{11} - \frac{C_{13}^2}{C_{33}} \tag{21}$$

$$C_{22}^{bulk,plane} = C_{22} - \frac{C_{12}^2}{C_{33}} \tag{22}$$

$$C_{12}^{bulk,plane} = C_{12} - \frac{C_{12}C_{13}}{C_{33}} \tag{23}$$

The relationship between the plane-stress elastic constants of the bulk and film models and the surface elastic constants is expressed by Eq. 24 [Izumi *et al.*, 2004], [Zare Pakzad *et al.*, 2021b], [Zare Pakzad *et al.*, 2023b]. To obtain elastic constants, infinitesimal strains are applied to the simulation box in different directions and the resulting variation of the energy is measured.

$$C_{ijkl}^{film,plane} = C_{ijkl}^{bulk,plane} - \frac{2}{L_z} d_{ijkl} \tag{24}$$

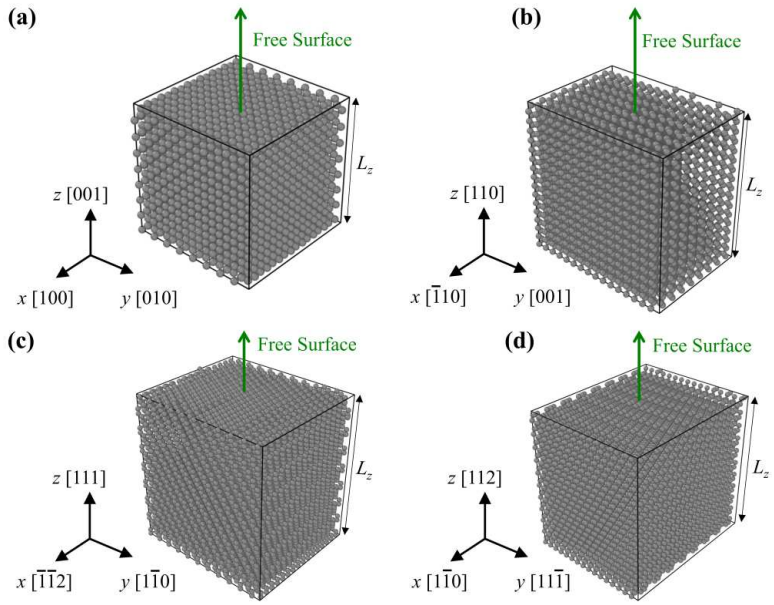

Fig. 3. The atomic structures used for calculating surface properties of unreconstructed Si thin films with different crystallographic orientations and associated free surfaces in the z-direction. The depicted structures correspond to Si orientations of (a) Si (100), (b) Si (110), (c) Si (111), and (d) Si (112).

3. Results

The section begins by establishing surface parameters, such as surface stresses and surface elastic constants, for different orientations of unreconstructed Si thin films (Section 3.1). Next, the bending simulation results for Si NWs modeled using MD with varying critical dimension and crystallographic orientations are presented in Section 3.2. Subsequently, the force-deflection relationships resulting from the simulations are examined to extract the modulus of elasticity of the Si NWs. The modulus of elasticity results are interpreted using different models from the existing literature (Section 3.3).

3.1. *Surface Properties of Si*

Despite numerous studies employing atomistic [Izumi *et al.*, 2004], [Park, 2008], [Pishkenari & Rezaei, 2017], [Xu & Kim, 2019], [Zare Pakzad *et al.*, 2021b], DFT [Lee & Rudd, 2007], [Melis *et al.*, 2015], [Melis *et al.*, 2016], [Jung & Shin, 2017], finite element [Quagliotti *et al.*, 2013], [Delph, 2008], [Payne *et al.*, 1989], [Miyamoto, 1994], [Alerhand *et al.*, 1988], and experimental [Pennelli *et al.*, 2012] approaches to investigate the surface constants of Si, a consensus regarding surface stress profiles and the subsequent calculation of constants for different crystalline orientations and surface conditions is lacking. A recent study has provided insights into the surface constants of unreconstructed and oxidized Si thin films offering valuable analysis regarding the surface properties of crystalline Si with different surface states [Zare Pakzad *et al.*, 2023b]. In line with that investigation, the unreconstructed Si thin films with (100), (110), (111), and (112) free surface orientations shown in Fig. 3 are examined for the calculation of surface properties including surface stresses, f_{11} and f_{22}, and surface elasticity constants, d_{11} and d_{22}. The methodology described in Section 2.4 is employed to analyze nanoscale Si thin films. The validity of this approach has been previously verified on various Si surfaces, including amorphous and unreconstructed structures, using different interatomic potentials. These previous studies, conducted through MD and DFT, have demonstrated good agreement with the results obtained from the current method [Shchipalov, 2000], [Miller & Shenoy, 2000].

To calculate surface stress, Eq. 19 is utilized, taking into account the film thickness (L_z), and the resulting planar surface stresses are presented in Table 2. Additionally, the surface elasticity constants are computed using Eq. 21, Eq. 22, and Eq. 23, with the values also provided in Table 2. The local stresses along the thin film structures are calculated using Eq. 18, considering the estimated atomic volume. The surface elastic constants are obtained for the film structures using limited thicknesses, while the bulk models are separately examined. Eq. 24, with the associated film thickness of L_z, is employed for this purpose. Table 2 further illustrates the average surface stress and surface elasticity constants for each orientation of the free surface. Remarkably, the obtained surface stress and surface elasticity constants for Si (100) and Si (110) crystal orientations align precisely with prior reports [Shchipalov, 2000], [Izumi *et al.*, 2004], [Pishkenari & Rezaei, 2017], [Zare Pakzad *et al.*, 2021b], [Zare Pakzad *et al.*, 2023b]. To the best of our knowledge, there is currently no existing study that provides surface constants for (111) and (112) Si thin films. The surface properties obtained here will be utilized in Section 3.2 to interpret the bending response of Si NWs using different surface formulations integrated into nanomechanical models. To confirm the results obtained here, stress-based [Izumi *et al.*, 2004] and energy-based [Miller & Shenoy, 2000] methods are employed to calculate the surface properties for different free surfaces of unreconstructed Si thin film. This ensures a high precision in determining the surface properties, thus verifying the relaxed state of the atomic configuration.

3.2. *Bending Response of Si NWs*

In Fig. 4 (a), the graph demonstrates the correlation between force and deflection ($F - w$) during a three-point bending test of a Si NW simulated using the MD method. Five significant deformation points (p_1 to p_5) are identified for detailed examination of the $F - w$ behavior, and accompanying snapshots of the bending deformation of the Si NW profile are presented in Fig. 4 (b). The gray shaded region (between points p_1 and p_2) depicted in Fig. 4 (a) represents the range of deformation occurring in the middle of the Si NW, reaching approximately $h/2$, before transitioning into non-linearity, indicating large deflection during Si NW deformation. Similarly, Fig. 4 (b) illustrates the deflection level attained at p_2 as the bending continues in the mid-section, eventually reaching the ultimate force level. The point p_3 exhibits the deviation observed between nanomechanical modeling and $F - w$ response given here. The ultimate force is also shown as point p_4. Finally, the fracture snapshot corresponding to Si NW failure is denoted as p_5. The response of the Si NW demonstrates a nonlinear relationship between force and displacement, covering a force range of up to 180 nN and a corresponding deflection range of up to 10 nm at the center of the NW. Examination of Si NWs with different crystal orientations and critical dimensions shows that incorporating surface properties like surface stresses and surface elastic constants (given in Table 2), along with intrinsic stresses, into the relevant models becomes essential to effectively apply various nanomechanical models for fitting the obtained $F - w$ responses. In this respect, MD simulations are utilized to determine the intrinsic stresses induced in Si NWs of different sizes and orientations. Once the relaxation process reaches a steady state, the atomic stresses along the longitudinal direction (x-axis) are computed for each Si NW using Eq. 18. The nonlinear response, combined with the expected large deformations in Si NWs, results in a clear change in the slope of the force-deflection curve once the deflections surpass a specific threshold, identified as point p_2 (half of the critical dimension) in Fig. 4 (a).

Table 3 presents the calculated surface-induced residual stresses for Si NWs with varying critical dimensions and orientations. In this study, it is assumed that the surface-induced residual stress represents the total intrinsic stress which will also be regarded as an initial tensile/compressive stress within the associated models. Intrinsic stresses in Si NWs have been reported in previous studies, including both

Table 2. Surface stress and surface elastic constants calculated for unreconstructed Si structures with associated crystallographic orientations.

Structure	Surface Stress (N/m)			Surface Elasticity (N/m)		
	f_{11}	f_{22}	f_{avg}	d_{11}	d_{22}	d_{avg}
Si (100)	-0.88	-0.88	-0.88	-8.77	-8.77	-8.77
Si (110)	-1.57	-0.95	-1.26	+3.40	-15.10	-5.85
Si (111)	-0.88	-1.23	-1.06	-18.67	+8.42	-5.12
Si (112)	-4.42	-2.11	-3.27	-25.10	+22.38	-1.36

computational [Zhan & Gu, 2012] and experimental [Calahorra *et al.*, 2015], [Dolabella *et al.*, 2020], [Spejo *et al.*, 2020], [Nasr Esfahani *et al.*, 2022], [Zare Pakzad *et al.*, 2023b] investigations. These studies have observed intrinsic stress values in Si NWs within a range of 100 MPa to 1.2 GPa. In particular, the intrinsic stress in Si NWs induced by the native oxide formation has been observed previously up to 1.2 GPa [Nasr Esfahani *et al.*, 2022]. The observed tensile stress state in unreconstructed Si NWs in the present study agrees with prior literature. However, conducting a direct comparison of the stress obtained in the simulations with experimental data might be challenging due to the lack of data specific for Si NWs with an unreconstructed surface state compared to native oxide [Nasr Esfahani *et al.*, 2022] or hydrogen passivated [Lee & Rudd, 2007] surface states.

The nanomechanical model fitting shown in Fig. 4 (a) corresponds to the ExtZP model, which is obtained by incorporating the relevant surface and intrinsic parameters. The detailed estimation of the modulus of elasticity for Si NWs with various dimensions and crystallographic orientations using nanomechanical models, as described in Section 2.1, is provided in Section 3.3. The comparison conducted in this study, using MD simulations on unreconstructed Si NWs modeled at 1.0 K, provide a comprehensive basis to evaluate the nanomechanical approaches. Additionally, further insights into room-temperature behavior and potential comparisons with experimental data can be explored in previous studies [Nasr Esfahani *et al.*, 2022], [Zare Pakzad *et al.*, 2023b]. The timescale difference [Kang & Cai, 2007], [Park *et al.*, 2008] between atomistic modeling and experimental approaches can be linked to the understanding of deformation mechanism and mechanical properties in Si NWs [Zare Pakzad *et al.*, 2023a], [Pakzad *et al.*, 2024]. In this respect, prior studies report minimal effects when employing dynamic and quasi-static loading techniques to explore mechanical properties in NWs [Liu & Shen, 2012]. The fracture behavior observed in Si NWs, as depicted in snapshots of Fig. 4 (b), indicates ruptures occurring near the support region, which can be attributed to large deformations commonly observed in Si NWs [Ngo *et al.*, 2006], [Zhan *et al.*, 2012].

Table 3. Intrinsic stresses of Si NWs with different critical dimensions and crystallographic orientations obtained via MD simulations.

Structure	Si Orientation			Intrinsic Stress (GPa)			
	x	y	z	$h = 2nm$	$h = 3nm$	$h = 4nm$	$h = 5nm$
Si $< 100 >$	[100]	[010]	[001]	0.69	0.51	0.53	0.38
Si $< 110 >$	[110]	[001]	$[\bar{1}10]$	1.87	1.46	1.23	0.77
Si $< 111 >$	[111]	$[1\bar{1}0]$	$[\bar{1}\bar{1}2]$	1.73	0.98	1.26	0.80
Si $< 112 >$	[112]	$[11\bar{1}]$	$[1\bar{1}0]$	1.48	0.81	1.05	0.65

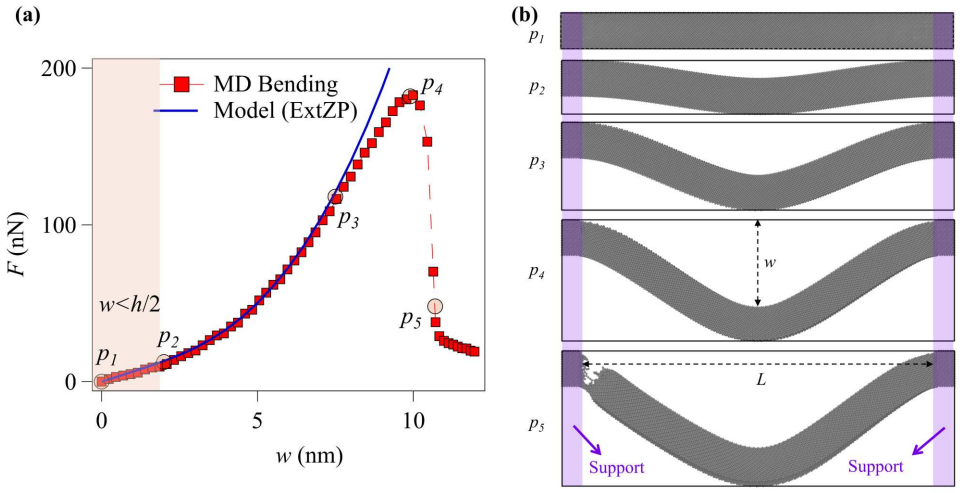

Fig. 4. (a) Force vs. deflection data obtained through 3-point bending simulation of a Si NW of $h = 4$ nm and fitted curve using the ExtZP model. (b) Atomic configurations of a Si NW and snapshots upon deformation of the Si NW during bending experiment.

3.3. *Interpretation of Results*

This section provides a detailed explanation of the interpretation of force-deflection responses for Si NWs with different dimensions and crystal orientations. Previous studies [Heidelberg *et al.*, 2006], [Zhan & Gu, 2012], [Zare Pakzad *et al.*, 2023b] have used a fitting procedure that begins with small deflections and extends to include progressively larger displacements. It is important to note that each nanomechanical model attributes the nonlinearity of the $F-w$ curve to different sets of parameters, including axial extension, intrinsic stress, and surface effects. Thus, each obtained $F-w$ curve is analyzed using five nanomechanical models, utilizing the appropriate input parameters, to obtain the modulus of elasticity of the Si NW. Among the models used, the ExtZP model is the comprehensive method that incorporates the surface stress (f_{11} and f_{22}) and surface elastic constants (d_{11} and d_{22}) provided in Table 2, as well as the intrinsic stresses given in Table 3, along with geometric details for interpreting the bending response. The SimpZP model considers the intrinsic stresses provided here as the initial tension (σ_0) and incorporates the surface properties f_{11} and d_{11} during the fitting procedure. The Zhan model relies on the previously given surface constants (f_{11} and d_{11}) without including any intrinsic terms. In contrast, the Hudson model includes the intrinsic term based on the initial tension adopted from Table 3, without incorporating any surface properties. Finally, the Heidelberg model performs the fitting procedure without including any surface or intrinsic terms. The bending rigidity formulations provided in Section 2.2 are utilized with the previously mentioned details specific to each nanomechanical model, taking advantage of the relevant surface properties. The procedure outlined

for estimating the modulus of elasticity using the provided models and the fitting curve shown in Fig. 4 (a) has been applied to Si NWs. The results are presented in Fig. 5 for different crystal orientations. Specifically, the modulus of elasticity estimation for $< 100 >$, $< 110 >$, $< 111 >$, and $< 112 >$-oriented Si NWs, with h ranging from 2.0 to 5.0 nm, is shown in Fig. 5 (a), (b), (c), and (d), respectively. The constant bulk moduli of elasticity presented in Fig. 5 (given as dashed lines) for different crystal orientations are extracted from experimental studies [Nasr Esfahani & Alaca, 2019]. These values are comparable to previously reported values obtained through computational approaches [Zare Pakzad *et al.*, 2023a]. Moreover, minor changes in trends as depicted in Fig. 5 are associated with the collective influences of surface properties and intrinsic stresses, although these deviations remain insignificant compared to the decrease in the elastic modulus observed at smaller dimensions.

The trend observed for Si NWs with varying crystal orientations is a decrease in the modulus of elasticity as the critical dimension h increases, though the rate of decrease varies depending on the orientation and the specific nanomechanical model employed. Specifically, for $< 100 >$-oriented Si NWs given in Fig. 5 (a), the modulus of elasticity estimation remains relatively constant for different critical dimensions, while incorporating the Heidelberg and Hudson models. When incorporating the surface and/or intrinsic terms in the Zhan, SimpZP, and ExtZP models, there is a consistent decreasing trend of E as the critical dimension h increases. The differences observed among these three models can be attributed to the utilization of distinct combinations of inputs, despite sharing a similar overall decreasing trend. For $< 110 >$-oriented Si NWs given in Fig. 5 (b), different decreasing trends are observable using the nanomechanical models. With the Heidelberg and Hudson model having higher estimation at 2.0 nm critical dimension, a similar constant trend is obtained with increase in h. However, the Zhan, SimpZP, and ExtZP models depict a decreasing E for Si NWs with increasing h.

Expanding the discussion to $< 111 >$-Si NWs, as shown in Fig. 5 (c), a clear decreasing trend of the modulus of elasticity can be observed for all the nanomechanical models used in this study. The estimations consistently demonstrate a similar trend when considering the effect of critical dimensions on the Si NWs. However, similar to the previous orientations, the Zhan, SimpZP, and ExtZP models yield higher estimations of E compared to the Heidelberg and Hudson models. For $< 112 >$-Si NWs, as shown in Fig. 5 (d), the trend of the modulus of elasticity also exhibits a similar decrease, but with differences between the models at each critical dimension. Once again, the Heidelberg and Hudson models provide lower estimations compared to the other three models. It is worth noting that the combination of parameters included in the nanomechanical models for the four crystal orientations studied here can result in differences of up to 100 GPa in the estimation of E, which is a significant variation. In particular, in the case of the smallest critical dimension (h of 2.0 nm), where surface effects are anticipated to exhibit a more sig-

nificant influence due to the size effect, models that encompass surface properties yield higher estimations, displaying more substantial deviations when contrasted with the Heidelberg and Hudson models. Notably, both the Heidelberg and Hudson models lack formulations that include surface-related terms, leading to inadequate estimations of the modulus of elasticity for Si NWs with critical dimensions below 10 nm. As the size increases, the surface contribution becomes less pronounced, leading to closer estimations among different models.

The discrepancy between different nanomechanical models becomes considerable in smaller dimensions (Fig. 5). The Heidelberg and Hudson nanomechanical models do not consider any surface effects such as surface stress and surface elastic constants. Hence, these methods have similar estimations for the elastic modulus. In contrast, Zhan, SimpZP, and ExtZP models illustrate the important effect of surface on the mechanical properties of Si nanostructures. Additionally, the discrepancies noted among these three models observed across different critical dimensions and crystal orientations highlight the impact of surface anisotropy. More specifically, when comparing the elastic modulus obtained for $< 100 >$ and $< 112 >$ Si NWs with a critical dimension of 2 nm, it becomes clear that smaller variations are expected among the Zhan, SimpZP, and ExtZP models for $< 100 >$-Si NWs, while differences exceeding 20 GPa are observed for $< 112 >$-Si NWs. This underscores the importance of anisotropic surface properties in interpreting elasticity in Si NWs. The minor variations observed in the modulus of elasticity are due to the surface effect in Si NWs, particularly the anisotropy in surface stresses and surface elastic constants.

In the investigation of size-dependent elastic properties of Si NWs, especially in cases of smaller dimensions, it becomes crucial to meticulously account for the inclusion of terms, particularly those relating to surface properties. When comparing the outcomes of the three models incorporating surface terms, it becomes apparent that both the Zhan and SimpZP models employ a common surface model known as the modified YL model. Depending on whether intrinsic terms are taken into account or not, divergences emerge between these two models. The Zhan model consistently yields higher estimates of the modulus of elasticity for all four orientations and critical dimensions. Conversely, the SimpZP model, which incorporates a tensile intrinsic stress during the fitting procedure, is anticipated to offer lower estimates of E depending on the critical dimension and the magnitude of the intrinsic stress. Furthermore, it is important to emphasize that among the four orientations studied in this work ($< 100 >$, $< 110 >$, $< 111 >$, $< 112 >$), only the ExtZP model benefits from the inclusion of anisotropic surface constants modeled via extended YL model given in Table 2. The remaining four models dismiss some or all of these surface terms, depending on their respective formulations. Previous findings emphasizing the significance of the native oxide surface state [Zare Pakzad *et al.*, 2021b], [Zare Pakzad *et al.*, 2023a], [Zare Pakzad *et al.*, 2023b], [Pakzad *et al.*, 2024], [Zare Pakzad *et al.*, 2024] can be extended via present study on unreconstructed Si

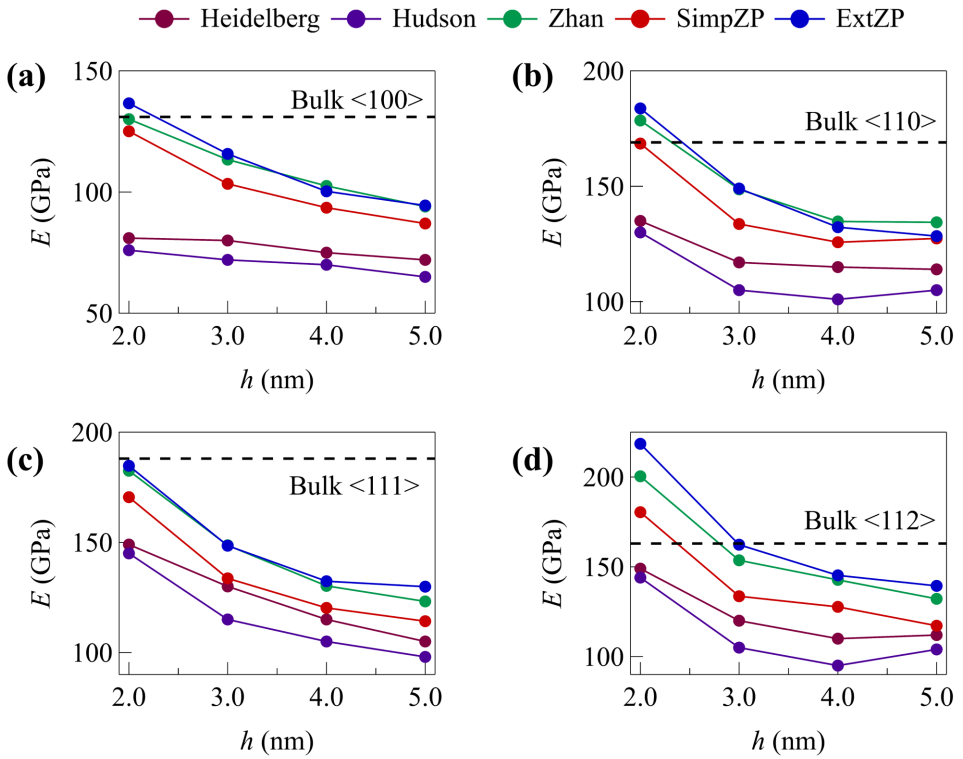

Fig. 5. : The modulus of elasticity estimations for Si NWs with (a) < 100 >, (b) < 110 >, (c) < 111 >, and (d) < 112 > crystal orientations. The Si NWs have different size in h ranging between 2 to 5 nm. The bulk modulus of elasticity for each orientation of Si is shown.

NWs. This highlights not only the importance of the surface state itself but also the anisotropic effects of surface properties. The selection of an appropriate model is crucial to avoid potential misinterpretations, as improper model selections may lead to misleading conclusions regarding the nature of unreconstructed Si surfaces and their impact on Si NW behavior. Given the discrepancies observed in the literature regarding experimental and computational estimations of the modulus of elasticity in Si NWs, the values obtained in this study are in line with the prior reports [Wang *et al.*, 2017], [Nasr Esfahani & Alaca, 2019], [Yang *et al.*, 2022], [Zare Pakzad *et al.*, 2023b]

4. Conclusion

This study exhibits the pivotal role that surface properties play in the mechanical behavior of Si NWs. By delving into the elastic properties of Si NWs with varying dimensions and crystal orientations through a diverse range of nanomechanical models, the intricate relationship between elastic properties, crystal orientation, and the chosen nanomechanical model has been unveiled. The analysis of force-deflection re-

sponses via MD simulations yields invaluable insights into the behavior of Si NWs at the nanoscale. These findings underscore the significance of meticulously modeling surface effects and incorporating anisotropic surface properties to attain a comprehensive grasp of Si NW mechanics. A thorough investigation into the accuracy and dependability of nanomechanical models requires considerations including geometrical aspects, environmental factors such as temperature, and consequent intrinsic stress and surface effects. To compare computational and experimental efforts, it is essential to meticulously consider factors such as the surface state (unreconstructed or native oxide) and environmental conditions, as well as other structural effects such as defects and flaws in materials. Additionally, the distinct trends observed in Si NWs with different crystal orientations emphasize the necessity of accounting for crystal orientation effects when examining their mechanical properties. This knowledge contributes to the ongoing exploration of size-dependent behaviors in Si NWs and enhances our comprehension of their surface attributes. A detailed comprehension of the effects originating from surface and crystal orientation aspects will expedite the development of more efficient and reliable NW-based technologies in the future.

Data Availability Statement

The data that support the findings of this study are available from the corresponding author upon reasonable request.

Conflict of Interest

The authors have no conflicts to disclose.

Acknowledgments

S.Z.P. and B.E.A. gratefully acknowledge financial support by Tubitak under grant no 120E347.

References

Akbari-Saatlu, M., Procek, M., Mattsson, C., Thungström, G., Nilsson, H.-E., Xiong, W., Xu, B., Li, Y., & Radamson, H. H. [2020] *Silicon nanowires for gas sensing: A review*, *Nanomaterials*, **10**(11), 2215.

Alaca, B. E. and Karimzadehkhouei, M. [2023] *Piezoresistive Nanowire-Based Electromechanical Sensors*, Reference Module in Biomedical Sciences, Vol. 3 (Encyclopedia of Sensors and Biosensors), pp. 555–566.

Alerhand, OL., Vanderbilt, D., Meade, R. D., & Joannopoulos, JD. [1988] *Spontaneous formation of stress domains on crystal surfaces*, *Physical Review Letters*, **61**(17), 1973.

Bachtold, A., Moser, J., & Dykman, M. I. [2022] *Mesoscopic Physics of Nanomechanical Systems*, *Reviews of Modern Physics*, **94**(4), 045005.

Calahorra, Y., Shtempluck, O., Kotchetkov, V., & Yaish, YE. [2015] *Young's modulus, residual stress, and crystal orientation of doubly clamped silicon nanowire beams*, *Nano letters*, **15**(5), 2945–2950.

Chen, T., Chiu, M., & Weng, C. [2006] *Derivation of the generalized Young-Laplace equation of curved interfaces in nanoscaled solids*, *Journal of Applied Physics*, **100**(7), 074308.

Delph, TJ. [2008] *Near-surface stresses in silicon (0 0 1)*, *Surface Science*, **602**(1), 259–267.

Dolabella, S., Frison, R., Chahine, G. A., Richter, C., Schulli, T. U., Tasdemir, Z., Alaca, B. E., Leblebici, Y., Dommann, A., & Neels, A. [2020] *Real-and Q-space travelling: multi-dimensional distribution maps of crystal-lattice strain ($\epsilon_0$44) and tilt of suspended monolithic silicon nanowire structures*, *Journal of applied crystallography*, **53**(1), 58–68.

Espinosa, H. D., Bernal, R. A., & Filleter, T. [2013] *In-Situ TEM Electromechanical Testing of Nanowires and Nanotubes*, *Nano and Cell Mechanics: Fundamentals and Frontiers*, 191–226.

Fedorov, S. A., Engelsen, N. J., Ghadimi, A. H., Bereyhi, M. J., Schilling, R., Wilson, D. J., & Kippenberg, T. J. [2019] *Generalized dissipation dilution in strained mechanical resonators*, *Physical Review B*, **99**(5), 054107.

Gurtin, M. E., & Murdoch, A. I. [1975] *A continuum theory of elastic material surfaces*, *Archive for Rational Mechanics and Analysis*, **57**(4), 291–323.

He, J., & Lilley, C. M. [2008] *Surface effect on the elastic behavior of static bending nanowires*, *Nano letters*, **8**(7), 1798–1802.

Heidelberg, A., Ngo, L. T., Wu, B., Phillips, M. A., Sharma, S., Kamins, T. I., Sader, J. E., & Boland, J. J. [2006] *A generalized description of the elastic properties of nanowires*, *Nano Letters*, **6**(6), 1101–1106.

Huang, J. and Zhang, Y. and Fan, A. and Li, Y. and Wang, H. and Ma, W. & Zhang, X. [2023] *Remarkable Thermal Conductivity Reduction of Silicon Nanowires during the Bending Process*, *ACS Applied Materials & Interfaces*, **15**(33), 39689–39696.

Hudson, S. D, Zhurov, V., Grbić, V., Grbić, M., & Hutter, J. L. [2013] *Measurement of the elastic modulus of spider mite silk fibers using atomic force microscopy*, *Journal of Applied Physics*, **113**(15), 154307.

Ilinov, A., & Kuronen, A. [2014] *Atomistic modeling of bending properties of oxidized silicon nanowires*, *Journal of Applied Physics*, **115**(10), 104305.

Izumi, S., Hara, S., Kumagai, T., & Sakai, S. [2004] *A method for calculating surface stress and surface elastic constants by molecular dynamics: application to the surface of crystal and amorphous silicon*, *Thin Solid Films*, **467**(1-2), 253–260.

Kang, K., & Cai, W. [2007] *Brittle and ductile fracture of semiconductor nanowires–molecular dynamics simulations*, *Philosophical Magazine*, **87**(14-15), 2169–2189.

Karimzadehkhouei, M., Ali, B., Jedari Ghourichaei, M., & Alaca, B. E. [2023] *Silicon Nanowires Driving Miniaturization of Microelectromechanical Systems Physical Sensors: A Review*, *Advanced Engineering Materials*, **25**(12), 2300007.

Kim, J. S., Park, S. H., Park, J. H., & Lee, J. S. [2006] *Molecular dynamics simulation of elastic properties of silicon nanocantilevers*, *Nanoscale and Microscale Thermophysical Engineering*, **10**(1), 55–65.

Lee, B., & Rudd, R. E. [2007] *First-principles study of the Young's modulus of Si¡001¿ nanowires*, *Physical Review B*, **75**(4), 041305.

Li, X., Yang, X., Zhang, Z., Wang, T., Sun, Y., Liu, Z., Li, X., Shi, Y., & Xu, J. [2021] *Impact of process fluctuations on reconfigurable silicon nanowire transistor*, *IEEE Transactions on Electron Devices*, **68**(2), 885–891.

Li, J., Lei, X., Ding, J., Gao, Z., Wang, H., & Shi, Y. [2022] *Surface effect on size dependent Young's modulus of nanowires: Exponentially decreased surface elasticity model*, *Materials Letters*, **307**, 131001.

Li, Q., Tan, X., & Yang, Y. [2023] *Sub-5 nm gate length selenium nanowire transistors: Implications for nanoelectronics*, *ACS Applied Nano Materials*, **6**(5), 4067–4077.

Liang, Y. and Qian, W. and Hu, R. and Gan, X. and Shi, S. and Li, Y. and Wang, J. and Liu, Z. and He, D. and Shi, Y. and Jun X. and Kunji C. & Linwei Y. [2023] *High-fidelity Moulding Growth and Cross-section Shaping of Ultrathin Monocrystalline Silicon Nanowires*, *Applied Surface Science*, **635**, 157635.

Liu, Q., & Shen, S. [2012] *On the large-strain plasticity of silicon nanowires: Effects of axial orientation and surface*, *International Journal of Plasticity*, **38**, 146–158. Elsevier.

Maita, F. and Maiolo, L. and Lucarini, I. and Del Rio De Vicente, J. I. and Sciortino, A. and Ledda, M. and Mussi, V. and Lisi, A. & Convertino, A. [2023] *Revealing Low Amplitude Signals of Neuroendocrine Cells through Disordered Silicon Nanowires-Based Microelectrode Array*, *Advanced Science*, **10**(24), 2301925.

Melis, Claudio, Colombo, Luciano, & Mana, Giovanni [2015] *Lattice strain at c-Si surfaces: a density functional theory calculation*, *Metrologia*, **52**(2), 214.

Melis, Claudio, Giordano, S, Colombo, Luciano, & Mana, G [2016] *Density functional theory calculations of the stress of oxidised (1 1 0) silicon surfaces*, *Metrologia*, **53**(6), 1339.

Miller, R.E., & Shenoy, V.B. [2000] *Size-dependent elastic properties of nanosized structural elements*, *Nanotechnology*, **11**(3), 139.

Miyamoto, Y. [1994] *Comparative study of Si (100) surface stresses with dimerized group-IV adatoms*, *Physical Review B*, **49**(3), 1947.

Momeni, K., Ji, Y., Wang, Y., Paul, S., Neshani, S., Yilmaz, D. E., Shin, Y. K., Zhang, D., Jiang, J.-W., Park, H. S., & others [2020] *Multiscale computational understanding and growth of 2D materials: a review*, *npj Computational Materials*, **6**(1), 22.

Müller, P., & Saúl, A. [2004] *Elastic effects on surface physics*, *Surface Science*

Reports, **54**(5-8), 157–258.

Nasr Esfahani, M., & Alaca, B.E. [2019] *A Review on Size-Dependent Mechanical Properties of Nanowires*, *Advanced Engineering Materials*, **21**(8), 1900192.

Nasr Esfahani, M., Zare Pakzad, S., Li, T., Li, X., Tasdemir, Z., Wollschläger, N., Leblebici, Y., & Alaca, B. E. [2022] *Effect of Native Oxide on Stress in Silicon Nanowires: Implications for Nanoelectromechanical Systems*, *ACS Applied Nano Materials*, **5**(9), 13276–13285.

Ngo, L. T., Almécija, D., Sader, J. E., Daly, B., Petkov, N., Holmes, J. D., Erts, D., & Boland, J. J. [2006] *Ultimate-strength germanium nanowires*, *Nano Letters*, **6**(12), 2964–2968.

Pakzad, S.Z., Nasr Esfahani, M., & Alaca, B.E. [2024] *Mechanical properties of silicon nanowires with native oxide surface state*, *Materials Today Communications*, **38**, 108321. Elsevier.

Panda, S., Hajra, S., Mistewicz, K., In-na, P., Sahu, M., Rajaitha, P. M., & Kim, H. J. [2022] *Piezoelectric energy harvesting systems for biomedical applications*, *Nano Energy*, **100**, 107514.

Park, SH, Kim, JS, Park, JH, Lee, JS, Choi, YK, & Kwon, OM [2005] *Molecular dynamics study on size-dependent elastic properties of silicon nanocantilevers*, *Thin Solid Films*, **492**(1-2), 285–289.

Park, H. S. [2008] *Surface stress effects on the resonant properties of silicon nanowires*, *Journal of Applied Physics*, **103**(12), 123504.

Payne, MC, Roberts, N, Needs, RJ, Needels, M, & Joannopoulos, JD. [1989] *Total energy and stress of metal and semiconductor surfaces*, *Surface Science*, **211**, 1–20.

Pennelli, G., Totaro, M., & Nannini, A. [2012] *Correlation between surface stress and apparent Young's modulus of top-down silicon nanowires*, *ACS nano*, **6**(12), 10727–10734.

Pishkenari, H. N., & Rezaei, S. [2017] *Characterization of silicon surface elastic constants based on different interatomic potentials*, *Thin Solid Films*, **626**, 104–109.

Plimpton, S. [1995] *Fast parallel algorithms for short-range molecular dynamics*, *Journal of Computational Physics*, **117**(1), 1–19.

Quagliotti, D., Mana, Giovanni, Massa, Enrico, Sasso, C., & Kuetgens, U. [2013] *A finite element analysis of surface-stress effects on measurement of the Si lattice parameter*, *Metrologia*, **50**(3), 243.

Shchipalov, Y.K. [2000] *Surface energy of crystalline and vitreous silica*, *Glass and Ceramics*, **57**(11), 374–377.

Song, F., Huang, G. L., Park, H. S., & Liu, X. N. [2011] *A continuum model for the mechanical behavior of nanowires including surface and surface-induced initial stresses*, *International Journal of Solids and Structures*, **48**(14-15), 2154–2163.

Spejo, L. B., Arrieta-Concha, J. L., Puydinger dos Santos, M. V., Barros, A. D., Bourdelle, K. K., Diniz, J. A., & Minamisawa, R. A. [2020] *Non-linear Ra-*

man shift-stress behavior in top-down fabricated highly strained silicon nanowires, *Journal of Applied Physics*, **128**(4), 045704.

Tersoff, J. [1988] *New empirical approach for the structure and energy of covalent systems*, *Physical review B*, **37**(12), 6991.

Ureña, F., Olsen, S. H., & Raskin, J.-P. [2013] *Raman measurements of uniaxial strain in silicon nanostructures*, *Journal of Applied Physics*, **114**(14), 144507.

Wang, G.-F., & Feng, X.-Q. [2007] *Effects of surface elasticity and residual surface tension on the natural frequency of microbeams*, *Applied Physics Letters*, **90**(23), 231904.

Wang, F., Dong, A., & Buhro, W. E. [2016] *Solution–liquid–solid synthesis, properties, and applications of one-dimensional colloidal semiconductor nanorods and nanowires*, *Chemical Reviews*, **116**(18), 10888–10933.

Wang, S., Shan, Z., & Huang, H. [2017] *The mechanical properties of nanowires*, *Advanced Science*, **4**(4), 1600332.

Xiao, Y., Shang, J., Kou, L. Z., & Li, C. [2022] *Surface deformation-dependent mechanical properties of bending nanowires: an ab initio core-shell model*, *Applied Mathematics and Mechanics*, **43**(2), 219–232.

Xu, X.-J., Wang, Y.-C., Wang, B., & Zhang, K. [2016] *A modified size-dependent core–shell model and its application in the wave propagation of square cellular networks*, *Physica E: Low-dimensional Systems and Nanostructures*, **80**, 53–61.

Xu, W., & Kim, W. K. [2019] *Molecular dynamics simulation of the uniaxial tensile test of silicon nanowires using the MEAM potential*, *Mechanics of Materials*, **137**, 103140.

Yaish, YE., Calahorra, Y., Shtempluck, O., & Kotchetkov, V. [2015] *Three-point bending analysis of doubly clamped silicon nanowire beams; Young's modulus, initial stress, and crystal orientation*, *Journal of Applied Physics*, **117**(16), 164311.

Yang, C. K., Van Der Drift, E. W. J. M., & French, P. J. [2022] *Review of scaling effects on physical properties and practicalities of cantilever sensors*, *Journal of Micromechanics and Microengineering*, **32**(10), 103002.

Yao, H., Yun, G., Bai, N., & Li, J. [2012] *Surface elasticity effect on the size-dependent elastic property of nanowires*, *Journal of Applied Physics*, **111**(8), 083506.

Ye, P., Ernst, T., & Khare, M. V. [2019] *The last silicon transistor: Nanosheet devices could be the final evolutionary step for Moore's Law*, *IEEE Spectrum*, **56**(8), 30–35.

Yokogawa, R., Hashimoto, S., Asada, S., Tomita, M., Watanabe, T., & Ogura, A. [2017] *Evaluation of controlled strain in silicon nanowire by UV Raman spectroscopy*, *Japanese Journal of Applied Physics*, **56**(6S1), 06GG10.

Zare Pakzad, S., Nasr Esfahani, M., Tasdemir, Z., Wollschlaeger, N., Li, X., Li, T., Yilmaz, M., Leblebici, Y., & Alaca, B. E. [2021] *A new characterization approach to study the mechanical behavior of silicon nanowires*, *Mrs Advances*, **6**(19), 500–505.

Zare Pakzad, S., Nasr Esfahani, M., & Alaca, B. E. [2021] "Molecular Dynamics Study of Orientation-dependent Tensile Properties of Si Nanowires with Native Oxide: Surface Stress and Surface Energy Effects," in *Proc. IEEE 21st International Conference on Nanotechnology (NANO)* (Montreal, QC, Canada), pp. 370–373.

Zare Pakzad, S., Nasr Esfahani, M., & Alaca, B. E. [2023] *The role of native oxide on the mechanical behavior of silicon nanowires*, *Materials Today Communications*, **34**, 105002.

Zare Pakzad, S., Nasr Esfahani, M., Tasdemir, Z., Wollschlager, N., Li, T., Li, X., Yilmaz, M., Leblebici, Y., & Alaca, B. E. [2023] *Nanomechanical Modeling of the Bending Response of Silicon Nanowires*, *ACS Applied Nano Materials*, **6**(17), 15465–15478.

Zare Pakzad, S., Akinci, S., Karimzadehkhouei, M., & Alaca, B. E. [2023] *Simplified top-down fabrication of sub-micron silicon nanowires*, *Semiconductor Science and Technology*, **38**(12), 125005.

Zare Pakzad, S., Ali, B., Coban, S. B., Karimzadehkhouei, M., & Alaca, B. E. [2023] "Innovative MEMS Stage for Automated Micromechanical Testing," in *Proc. IEEE 2023 International Conference on Manipulation, Automation and Robotics at Small Scales (MARSS)* (Abu Dhabi, UAE), pp. 1–6.

Zare Pakzad, S., Nasr Esfahani, M., Canadinc, D., & Alaca, B. E. [2024] *Machine Learning Insights into the Elasticity of Bottom-Up Silicon Nanowires*, *Preprint Available at SSRN*, 4791813.

Zhan, HF., & Gu, Y. [2012] *Modified beam theories for bending properties of nanowires considering surface/intrinsic effects and axial extension effect*, *Journal of applied physics*, **111**(8), 084305.

Zhang, A., Lee, J.-H., & Lieber, C. M. [2021] *Nanowire-enabled bioelectronics*, *Nano Today*, **38**, 101135.

Zhuo, XR, & Beom, HG [2018] *Atomistic study of the bending properties of silicon nanowires*, *Computational Materials Science*, **152**, 331–336.

Zimmerman, J.A., Webb III., E.B., Hoyt, J.J., Jones, R.E., Klein, P.A., & Bammann, D.J. [2004] *Calculation of stress in atomistic simulation*, *Modelling and Simulation in Materials Science and Engineering*, **12**(4), S319.

Manuscript Highlighted